LASER & PHOTONICS REVIEWS
www.lpr-journal.org

Deterministic Parity-Time Symmetry Single-Mode Oscillation in Filterless Multimode Resonators

Huashan Yang, Shifeng Liu, Mingzhen Liu, Peng Liu, Hao Zhang, Jijun He, and Shilong Pan**

Parity-time symmetry has great potential for mode selection in multimode resonators. However, in a PT-symmetry system with saturable absorption mechanisms, the random background noise can initiate single-mode oscillation at any of the maxima within the gain spectrum, that is, potential PT frequencies. Such randomness impedes the acquisition of high-quality signals at desired frequencies. Here, this work proposes a method to obtain deterministic PT-symmetry single-mode oscillation in a filterless multimode resonator through one-shot injection. With this technique, this work changes the system's gain spectrum and enhances the gain discrepancy. Utilizing the frequency domain saturable absorption of the resonator, oscillation at desired mode can maintain its frequency after the withdrawal of the injection signal. To validate the concept, this work establishes a polarization-division multiplexed dual-loop optoelectronic oscillator (OEO) with a 1-km long cavity operated under PT-symmetry conditions. By one-shot injecting the PT-OEO, this work effectively eliminates the randomness arising from the relatively flat gain spectrum, facilitating oscillation at any desired potential PT frequencies from 1.8 to 9 GHz without requiring elaborate frequency tuning structures. Moreover, the one-shot injection technique produces ultra-low phase noise performance, achieving a remarkable −158.6 dBc Hz^{-1}@10 kHz. This performance level stands in close comparison with the best phase noise values recorded for OEOs.

1. Introduction

Parity-time (PT) symmetry is a fundamental concept in physics that describes systems governed by non-Hermitian Hamiltonians, yet still exhibit eigenstates with real eigenvalues. When the PT-symmetry breaking condition occurs, the system manifests a pair of conjugate eigenvalues. PT-symmetry theory was first proposed in the field of quantum mechanics by Carl Bender and Steffan Boettcher in 1998.[1] Afterward, the exploration of PT-symmetry and its breaking phenomena was extended to optical platforms. This is due to the mathematically homologous of Maxwell's equations and the Schrödinger equation, which facilitates the realization of PT-symmetry by manipulating the gain and loss within coupled photonic structures.[2] In addition, the PT-symmetry breaking process exacerbates mode competition, thereby enabling single-mode oscillation in multimode resonators. Initially observed in a waveguide coupler,[3] PT-symmetry has since found applications in various optical and electrical resonators, including microring lasers,[4–6] microresonators,[7–11] active RLC circuits,[12] and optoelectronic oscillators (OEOs).[13–22] However, the presence of a heterogeneous gain spectrum in photonic resonators increases the randomness of the eigenfrequency of PT-symmetry breaking. Eigenfrequencies with comparable gains are frequent and unavoidable, leading to the potential for oscillations to randomly initiate at any of these frequencies. The initiated oscillation tends to persist due to the saturable absorption effect, a phenomenon prevalent in various photonic resonators such as quantum-dot mode-locked lasers,[23] fiber lasers,[24] and Q-switching lasers.[25] Consequently, achieving oscillation at a specific frequency on demand presents a significant challenge.

In this work, we propose a method to eliminate the inherent randomness in a PT-symmetric system by employing a *one-shot* injection process, enabling precise oscillation at desired Eigenfrequencies. External injection of a stable periodic signal into an oscillator is a widely employed technique in both photonics and microwave fields, which has proven effective in enhancing the performance of various oscillators, including solid-state microwave oscillators,[26] semiconductor lasers,[27,28] OEOs,[29] and dissipative Kerr soliton (DKS) combs.[30] A critical aspect of this technique is that the injected signal must persist throughout the oscillator's operation to maintain performance enhancement.[31,32] Unlike previous works, our injection process effectively modifies the gain spectrum of the PT-symmetric system, providing

H. Yang, S. Liu, M. Liu, P. Liu, H. Zhang, J. He, S. Pan
National Key Laboratory of Microwave Photonics
Nanjing University of Aeronautics and Astronautics
Nanjing 211106, China
E-mail: jijun.he@nuaa.edu.cn; pans@nuaa.edu.cn
J. He
Key Laboratory of Aerospace Integrated Circuits and Microsystem
Ministry of Industry and Information Technology
Nanjing 211106, China

The ORCID identification number(s) for the author(s) of this article can be found under https://doi.org/10.1002/lpor.202400913

DOI: 10.1002/lpor.202400913

stable additional gain to the desired eigenmode only during the initiation stage. The seed signal generated at the desired eigenmode by the one-shot injection is sustained by the saturable absorption effect within the system. To validate the concept, we establish a polarization-division multiplexed dual-loop OEO. The OEO, featuring identical loop lengths and opposite gains, is realized through a polarization-division multiplexed structure employing two optical tunable delay lines (OTDLs).

Both theoretical and experimental results demonstrate that the oscillation frequency of a PT-OEO without injection may randomly occur at any of the multiple maxima in the gain spectrum, referred to as potential PT frequencies. In contrast, our proposed deterministic PT-OEO can reliably oscillate at any definite potential PT frequencies ranging from 1.8 to 9 GHz with the assistance of a one-shot injection signal. The oscillation frequency can sustain itself after the withdrawal of the injection signal, owing to the frequency domain saturable absorption mechanism inherent within the PT-OEO. Without interference from the injection signal, the deterministic PT-OEO exhibits favorable phase noise performance, achieving −158.6 dBc Hz^{-1} at 10-kHz offset with just 4.4-km optical fiber in the cavity. This achievement closely rivals the best phase noise record observed in OEOs.[33] Additionally, a decent side-mode suppression ratio (SMSR) of 63.8 dB is achieved through the PT-symmetry regime. These findings not only expand the application scope of the injection locking technique but also contribute to a deeper understanding of the injection locking mechanism across various platforms. Moreover, due to the reciprocity between the time domain and frequency domain, our work may stimulate innovative approaches for enhancing the performance of PT-symmetry oscillators, which opens up possibilities for novel concepts such as mutual injection of PT-symmetry optical systems and synchronization of different PT-symmetry optical resonators like quantum dot mode-locked lasers,[23] fiber lasers,[24] and Q-switching lasers.[25]

2. Results

2.1. Principle of the Deterministic PT-OEO

Figure 1a illustrates the conceptual principle for the deterministic PT-OEO. In a traditional filterless PT-OEO, the PT-symmetry process can amplify the ripples in the gain spectrum γ_n into a sharpened gain spectrum reminiscent of a multi-passband filter with a new gain spectrum g_n. Single-mode oscillation is enabled by the enlarged gain difference in the new gain spectrum under PT-symmetry $g_n = \sqrt{\gamma_n'^2 - \kappa^2}$(see Methods). Unfortunately, the oscillation frequency of an actual PT-OEO cannot be arbitrarily selected from the passband frequencies of the multi-passband filter formed by PT-symmetry because of the frequency domain saturable absorption induced by the Mach-Zehnder modulator (MZM). Since the system involves massive modes across a wide spectral range, we take a simplified case as an example to elucidate the randomness in a conventional PT-OEO. As depicted in Figure 1a, two potential PT frequencies exist, with comparable gains at the i_{th} and j_{th} modes within the narrow spectral range. Given a relatively potent initial noise signal positioned at the j_{th} mode (lower peak), the signal is rapidly amplified to the saturation level after a few loops. Conversely, the noise signal at the i_{th} mode (higher peak) gets suppressed due to the saturable absorption induced by the MZM. Suppose the MZM is biased at the quadrature point, the electrical field of the output signal of the MZM is given by

$$x_{out}(t) \propto A_i \cos(\omega_i t) + A_j \cos(\omega_j t) \tag{1}$$

where $A_i = J_0(\beta_j)J_1(\beta_i)$ and $A_j = J_0(\beta_i)J_1(\beta_j)$ represent the amplitudes of each signal, respectively. $\beta_i = 2\pi V_i/V_\pi$ and $\beta_j = 2\pi V_j/V_\pi$ are the modulation indices of the electrical signal at the i_{th} and j_{th} peaks, respectively. V_i, V_j and ω_i, ω_j are their voltages and angular frequencies, respectively, and V_π is the half-wave voltage of the MZM (see Methods). Substituting $\beta_i \to 0$ and $\beta_j \to \pi/2$ (the saturation point of the MZM) into A_i and A_j, we find that the amplitude of the weaker signal at ω_i would be suppressed by ≈35% compared to the stronger signal ω_j. This mechanism resembles the saturable absorption observed in mode-locked lasers,[34] with the distinction being that saturation occurs in the frequency domain. Since the filterless PT-OEO exhibits a relatively flat gain spectrum, the gain difference between different peaks is not prominent. After passing through the amplification part of the PT-OEO, we have

$$\frac{G_{PT,j}}{G_{PT,i}} > \frac{A_i}{A_j} \cdot \frac{\beta_j}{\beta_i} \approx 0.65 \tag{2}$$

where $G_{PT,i}$ and $G_{PT,j}$ are the dimensionless loop voltage gains of each mode of the PT-OEO, respectively. Equation (2) illustrates that the noise at the i_{th} mode (higher peak) can be sufficiently suppressed by the frequency domain saturable absorption mechanism if single-mode oscillation is initiated at a peak with a gain exceeding half of the maximum gain. Single-mode oscillation at this mode can be sustained if there are no significant environmental fluctuations. In the case that the oscillation is initiated at the i_{th} mode with the highest gain, Equation (2) is still satisfied by exchanging i and j. In an actual PT-OEO, numerous gain peaks satisfy Equation (2), referred to as potential PT frequencies. Consequently, the oscillation frequency of a PT-OEO can randomly be one of the multiple potential PT frequencies.

Deterministic oscillation of the PT-O can be achieved with a one-shot injection signal. We introduce a very weak injection signal at the j_{th} mode (lower peak). Despite its low power, the injection signal surpasses the background noise level, resulting in a prominent gain peak during the initial stage of the oscillation. In addition, the injection signal serves as an effective seed signal at the desired frequency. Consequently, the signal amplitude at the j_{th} mode undergoes rapid escalation, eventually reaching the system's saturation power. Given that the injection power is notably lower than the amplifier saturation power, the total output microwave power of the PT-OEO does not experience a significant decrease after the injection is turned off. Although the small signal gain of the other peak is higher than the selected j_{th} mode, the signal amplitude at this mode is too low to distinguish itself from the noise floor due to the frequency domain saturable absorption mechanism induced by the MZM, as described in Equation (2).

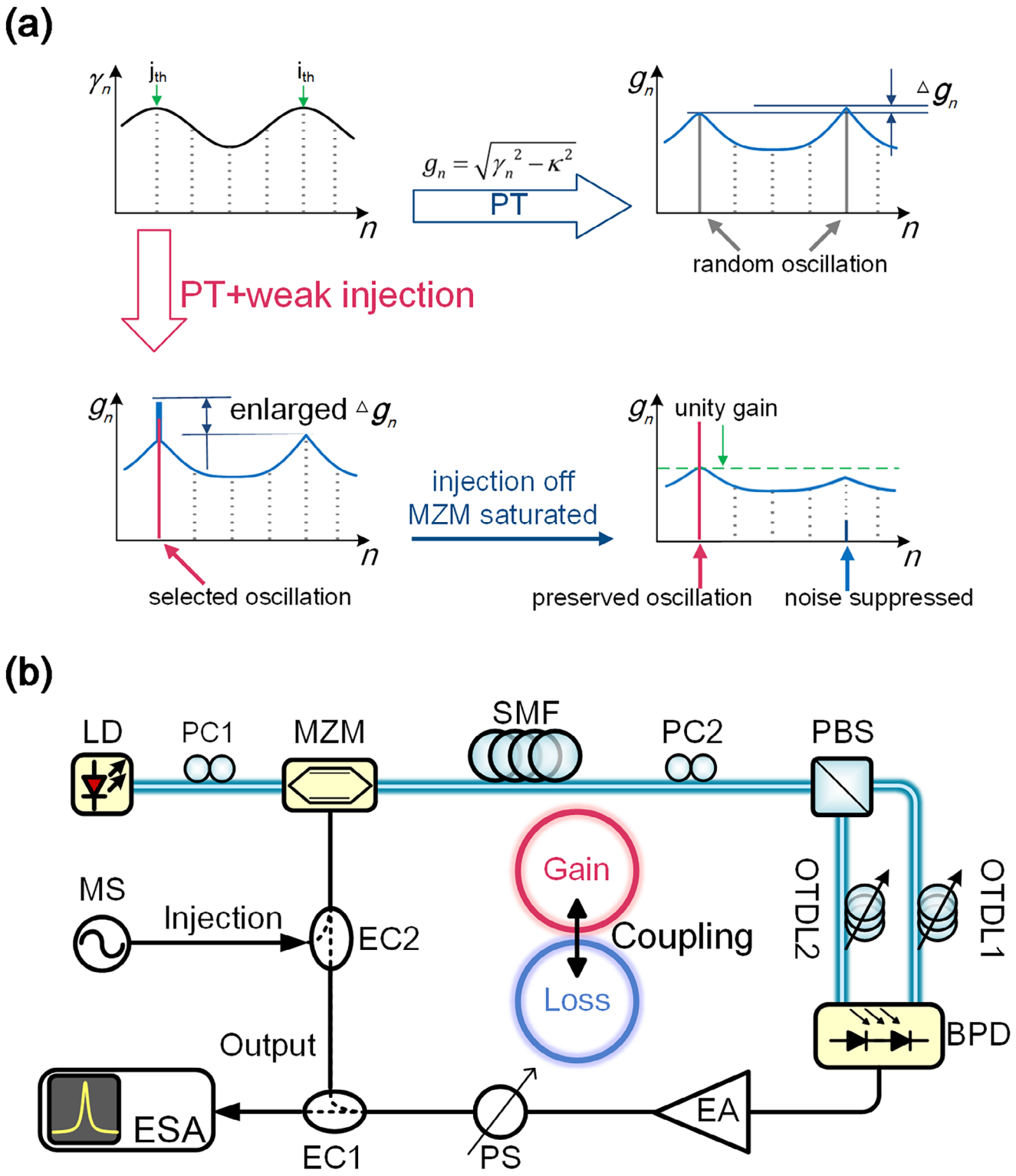

Figure 1. a) Principle of the PT-symmetry system under external injection. The injection locking process enlarges the gain difference between the selected mode and the other modes, thereby steering the system toward the intended oscillation frequency. Upon discontinuation of the injection, the oscillation frequency can sustain itself, thanks to the frequency domain saturable absorption mechanism of the MZM. The dashed lines indicate the spectral positions of the cavity modes. b) Experimental setup of the injection-locked PT-OEO. LD, laser diode; PC, polarization controller; MZM, Mach-Zehnder modulator; SMF, single-mode fiber; PBS, polarization beam splitter; OTDL, optical tunable delay line; BPD, balanced photodetector; EA, electrical amplifier; PS, phase shifter; EC, electrical coupler; MS, microwave source; ESA, electrical spectrum analyzer.

2.2. Simulation and Experimental Verification

To experimentally investigate the properties of PT-symmetry in the injection regime, we build a PT-OEO, as shown in Figure 1b. A continuous light wave generated by a laser diode (G&H EM650) is directed to an MZM (iXblue MXAN-LM-20), with its polarization direction tuned by PC1 to minimize the polarization-dependent loss. After passing through a length of single-mode fiber (SMF), the optical signal is split into two paths by a PBS. The PBS, together with another PC (PC2) and two optical tunable delay lines (OTDLs) labeled as OTDL1 and OTDL2, serve to adjust the optical power splitting ratio and the time delay of the two paths, respectively, to satisfy the PT-symmetry condition in the OEO. The SMF is placed in a thermostatic chamber,[35] ensuring that the optical fiber undergoes less than 5 mm of change in the steady state, which helps maintain the frequency stability of the generated signal. A BPD (Discovery DCS40s) combines the two paths and performs optical-to-electrical conversion. Following electrical amplification (CETC WFB9158H) and phase shifting, 10% of the microwave power is directed to an electrical spectrum analyzer (ESA, Rohde & Schwarz FSWP) for analyzing the electrical spectrum and phase noise of the OEO. A phase shifter (PS) compensates for the phase shift in the mutual loop induced by OTDL1, OTDL2, and PC2. The injection locking process is facilitated by injecting a microwave signal generated by a microwave source (MS, Agilent E8257D). A 3-dB coupler (EC2) combines the injection and oscillation signals and feeds them to the MZM.

First, a PT-OEO with 1 km SMF is built. The MS is connected to EC2 with the injection signal turned off to ensure the cavity's physical properties are not altered. Keeping the cavity unchanged, we restart the OEO twenty times. The advantage of PT-symmetry is evident as single-mode oscillation can be readily achieved without the need for RF or photonic filters. However, we observe nine different frequencies ranging from 1.8 to 9.0 GHz. The electrical spectra and their center frequencies are detailed in **Figure 2**a. The mode spacing is ≈200 kHz, as depicted by the blue lines in **Figure 3**c,d, which matches well with the loop delay, indicating the absence of Vernier effect in the cavity. Since there is no microwave filter in the OEO loop, the spectrum of the 1.8 GHz oscillation exhibits multiple high-order harmonics. It should be noted that the sudden change in the noise floor at ≈5.5 GHz is attributed to the frequency response characteristic of the ESA.

To reproduce the observed behavior in the experiment and understand the underlying mechanism, we carry out a simulation using a model adapted from[36] (see Methods). Figure 2c illustrates the frequency response and the spectrum evolution of a hypothetic filterless single-loop OEO with only two very weak ripples. In each roundtrip, numerous modes undergo similar amplification, resulting in messy multimode oscillation, as depicted in Figure 2b. However, only frequencies at the peaks of H_n have the possibility of becoming dominant frequencies. The final spectrum, shown in the inset of Figure 2c, mirrors the spectral shape of H_n. PT-symmetry is then introduced, as depicted in Figure 2d–f. By applying Equation (6), the small ripples in Figure 2b are amplified to form a transmission spectrum with a sharp peak and a lower peak with a transmission of 0.8, as shown in Figure 2d. The OEO can achieve single-mode oscillation with the assistance of the steep transmission roll-off induced by PT symmetry. However, the oscillation frequency can be randomly located at either peak, as illustrated in Figure 2e,f. This is because the random fluctuation of the background noise and the gain spectrum could result in a stronger seed signal on either peak. Following a few loops of amplification, this seed signal tends to dominate as the primary oscillation mode signal due to the frequency domain saturable absorption mechanism induced by the MZM, even if it originates from the lower peak.

Deterministic oscillation frequency can be realized using the one-shot injection technique. **Figure 3**a) illustrates the dynamics of this technique through simulation. We employed the same simulation parameters as in Figure 2e–g and added a 0-dBm RF injection on the lower peak of H_n. Figure 3a demonstrates that the oscillation mode can be precisely located at the injected mode. The injection power significantly sharpens the gain spectrum of the OEO, resulting in high frequency purity. Subsequently, the external injection is turned off at the 501th roundtrip to simulate the scenario depicted in Figure 3a, and the oscillating mode remains located at the injected mode due to the PT-symmetry process. The PT-symmetry process suppresses most side modes, providing limited possible oscillation modes with sufficient gain for single-mode oscillation. The amplitudes of the side modes and the noisy modes increase, deteriorating the frequency purity, as shown in the lower inset of Figure 3a. Nevertheless, the previously injected mode retains almost the largest gain and amplitude, thanks to the frequency domain saturable absorption mechanism, as shown in Equation (2). To address the role of the saturable absorption of MZM and PT symmetry in the deterministic OEO dynamics, additional simulations demonstrate that both of them are essential for achieving a stable deterministic oscillation (see Supporting Information). Additionally, there is a substantial range of injection power and gain ripple tolerance for the deterministic PT-OEO (see Supporting Information). Therefore, despite the absence of the injection signal, the inherent randomness in the PT-symmetry process is eliminated by the injection process, enabling the system to maintain the desired oscillation frequency.

In the experiment, the power of the one-shot injection signal from the MS is set to 0 dBm. Unlike the random oscillation frequency of the classic PT-OEO, the one-shot injected PT-OEO exhibits deterministic oscillation frequency. By adjusting the injection frequency, the OEO can operate at any of the nine frequencies listed in Figure 2a. The close-in spectra of the injected and the non-injected PT-OEO at two different frequencies are shown in Figure 3c,d. In the injection regime, the 0-dBm microwave signal injection at each frequency pulls the random oscillation frequencies to the injected mode, resulting in a higher SMSR of more than 90 dB (red line in Figure 3c,d) owing to the sharper gain spectrum under external injection. Upon turning off the injection signal, the oscillating signal persists in the PT-OEO cavity, maintaining the oscillation frequency at the same gain peak. Since the PT-symmetry provides a rough filter effect, enabling the PT-OEO to continue operating without degenerating into multimode oscillation.

The frequency of the PT-OEO can be tuned simply by a one-shot injection with a new frequency and restarting the electrical amplifier. In Figure 3b, the initial oscillation frequency is defined by a one-shot injection signal at 7.1 GHz. Then, it can be switched to 7.9 GHz and back to 7.1 GHz via two one-shot injection pro-

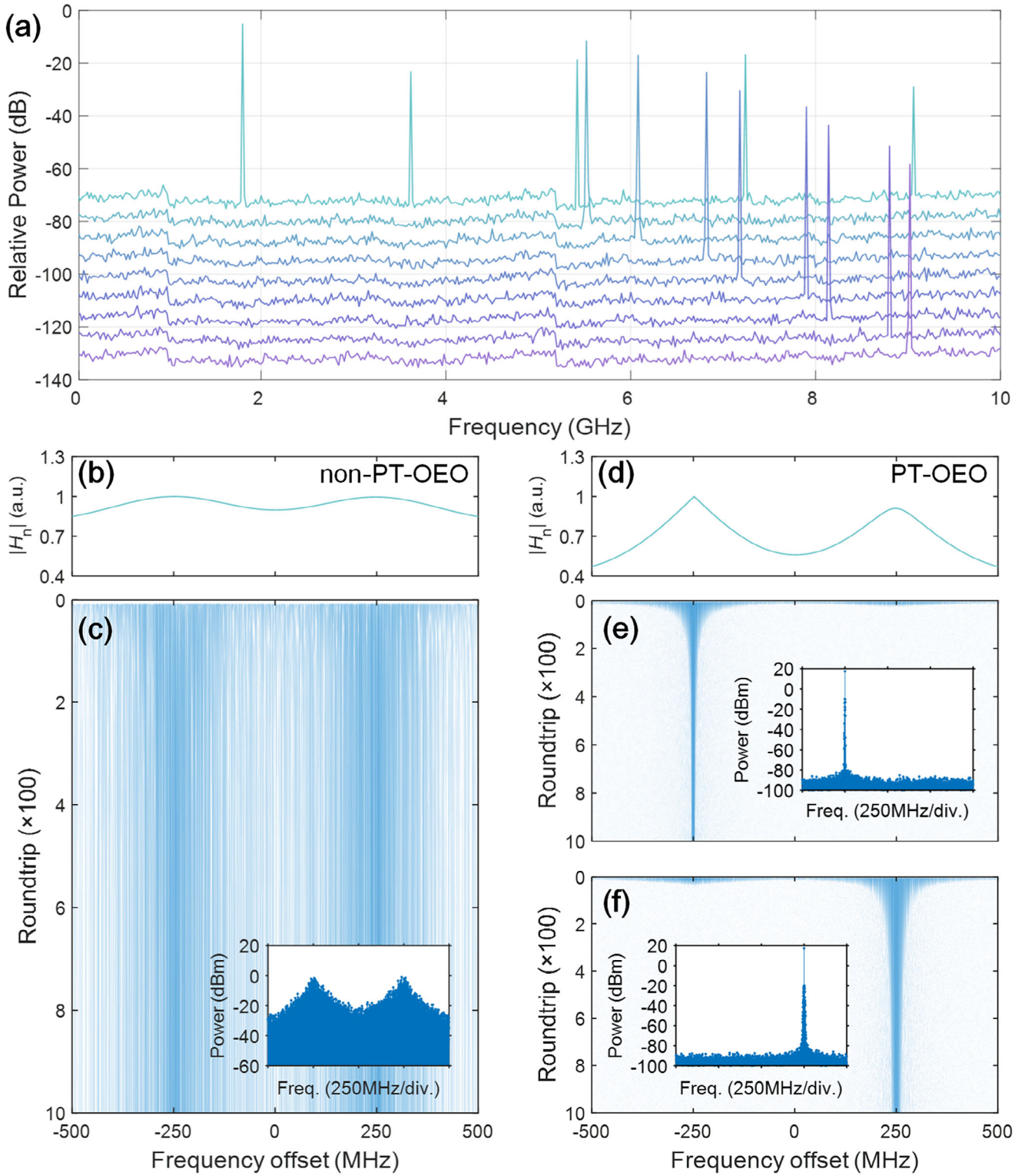

Figure 2. a) The measured electrical spectra of PT-OEO without injection signal. Nine different random frequencies are obtained. Each spectrum is offset to differentiate it from the others. b) Simulated frequency response of a hypothetic filterless single-loop OEO with only two very weak ripples. c) Simulated spectrum evolution of the OEO in (b), indicating the inability to establish single mode oscillation. Inset: the spectrum at the last roundtrip. d) Simulated frequency response of a PT-OEO calculated from (b). e,f) Simulated spectrum evolution of the PT-OEO in (d), showing that the oscillation can occur at either one of the peaks. Insets: spectra at the last roundtrip for each case.

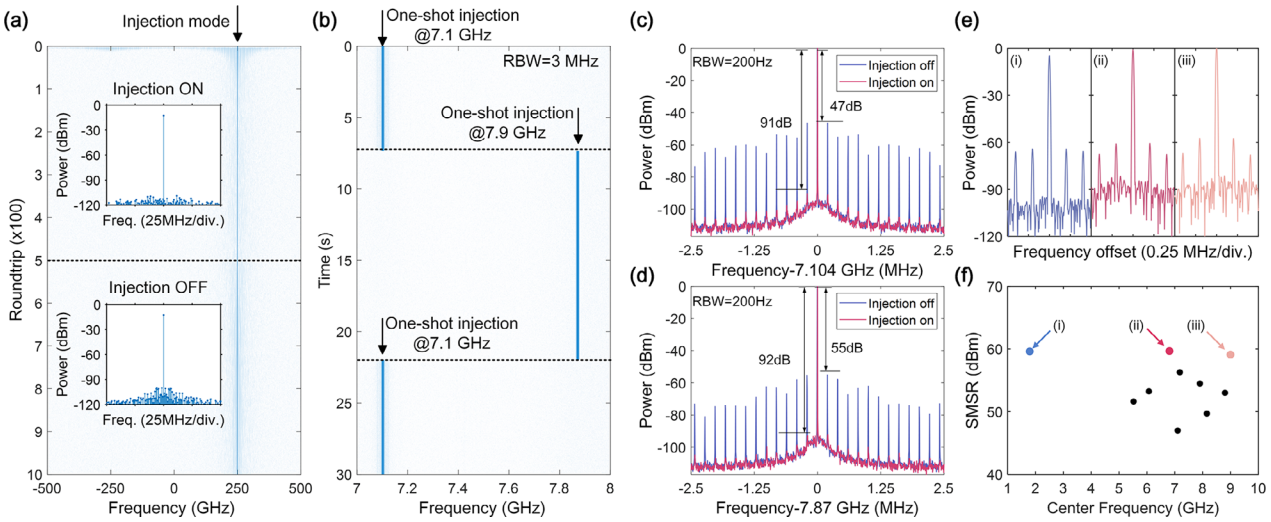

Figure 3. The PT-OEO with deterministic oscillation frequency enabled by one-shot injection. a) Simulated evolution of the spectrum for the injected PT-OEO. The oscillation frequency can be precisely located at the injected mode, and single mode oscillation persists after the injection signal is turned off. Insets: the spectra at the 500th roundtrip and the 1000th roundtrip. b) Measured spectrum evolution of the PT-OEO. The initial oscillation frequency is defined by a one-shot injection signal at 7.1 GHz. The oscillation frequency can be switched to 7.9 GHz and back to 7.1 GHz with the one-shot injection technique. c,d) Measured electrical spectra of the PT-OEO with and without injection signals at 7.104 and 7.87 GHz, respectively. e) Measured electrical spectra of the deterministic PT-OEO at 1.81, 6.81, and 9.01 GHz, respectively. f) Measured SMSR of the deterministic PT-OEO at different oscillation frequencies.

cesses. After injection withdrawal, the SMSR decreases to 47 and 55 dB, respectively, similar to the results without injection. This similarity in SMSR can be attributed to the fact that the gain spectrum remains unchanged before and after the one-shot injection. We notice that there is a large SMSR difference, so the SMSR of all potential PT-frequencies is measured, which varies from 47 to 60 dB, as shown in Figure 3f. This discrepancy in SMSR can be interpreted as indicative of the sharpness of the gain spectrum of the open-loop OEO. Figures 3e display the electrical spectra of the oscillation signals at 1.81, 6.81, and 9.01 GHz, respectively, which exhibit SMSRs over 60 dB. Although the injection locking technique is known to enhance the frequency stability of OEOs, our deterministic PT-OEO demonstrates stability for at least 3 min and a frequency fluctuation of less than ±1.2 kHz even in the absence of an injection signal (see Supporting Information).

2.3. Deterministic PT-OEOs with Ultra-Low Phase Noise

The one-shot injection technique offers the advantage that the output signal of the OEO is not degraded by the injection signal, allowing the use of an injection signal with poor phase noise. To validate the merits of our proposed method, we construct two ultra-low phase noise PT-OEOs using optical fibers of lengths 1 and 4.4 km, respectively. In order to mitigate the in-loop active noises of the OEOs, we employ high-performance optical and electrical components.[37] Additionally, we encase the glue-consolidated optical fiber coils in chambers isolated from acoustic and thermal disturbances,[35] and incorporate temperature feedback systems to minimize noise arising from ambient factors. Nonlinear effects within the optical fiber cavities are mitigated by reducing optical reflection, achieved through the incorporation of optical isolators within the OEOs and the connection of optical fiber cavities and other optical devices via fiber fusion. Similarly, microwave isolators are utilized to suppress reflections within the electrical paths. Both configurations of PT-OEO achieve three deterministic oscillations at frequencies of 7.7, 8.2, and 8.7 GHz, as depicted in **Figure** 4a–f. The PT-OEO with a 1 km optical fiber demonstrates improved SMSRs of 63.4, 63.8, and 62.9 dB, respectively, thanks to our noise suppression and fiber stabilization techniques. Similarly, the PT-OEO with a 4.4 km optical fiber also exhibits decent SMSRs of 51.8, 53.4, and 52 dB, respectively. In the absence of the injection signal, both deterministic PT-OEO configurations maintain favorable phase noise performances across the three oscillation frequencies. Figure 4g,h illustrate the phase noises of the injected PT-OEO, the non-injected PT-OEO, and the injection signal. In the case of the 1 km optical fiber, our proposed deterministic non-injected PT-OEO exhibits significantly lower phase noise compared to the injection signal across almost the entire offset frequency range. For instance, the phase noise of the 7.7 GHz signal at a 10 kHz frequency offset reaches −148 dBc Hz^{-1}, which is 32 dB lower than that of the injection signal. Conversely, the injected PT-OEO showcases poorer phase noise performance of −138 dBc Hz^{-1} at 10 kHz due to the higher phase noise of the injection signal. In the 4.4 km case, the proposed PT-OEO at 8.7 GHz exhibits a phase noise of −156 dBc Hz^{-1} at a 10 kHz frequency offset, which is 8 dB lower than the injected OEO. The improvement in phase noise is even more significant at lower frequency offsets in the 4.4 km case, as depicted in Figure 4h. For instance, the phase noises are −125 and −109 dBc Hz^{-1} at 1 kHz frequency offset for the non-injected and injected PT-OEOs, respectively. The phase noises of the two deterministic PT-OEOs at different frequencies exhibit a considerable degree of similarity, as shown in Figure 4i,j. In the 1 km case, the phase noises are −121.2, −120.3, and −120.8 dBc Hz^{-1} at 1 kHz frequency offset, and −145.9, −149.9, and −148.6 dBc Hz^{-1} at 10 kHz frequency off-

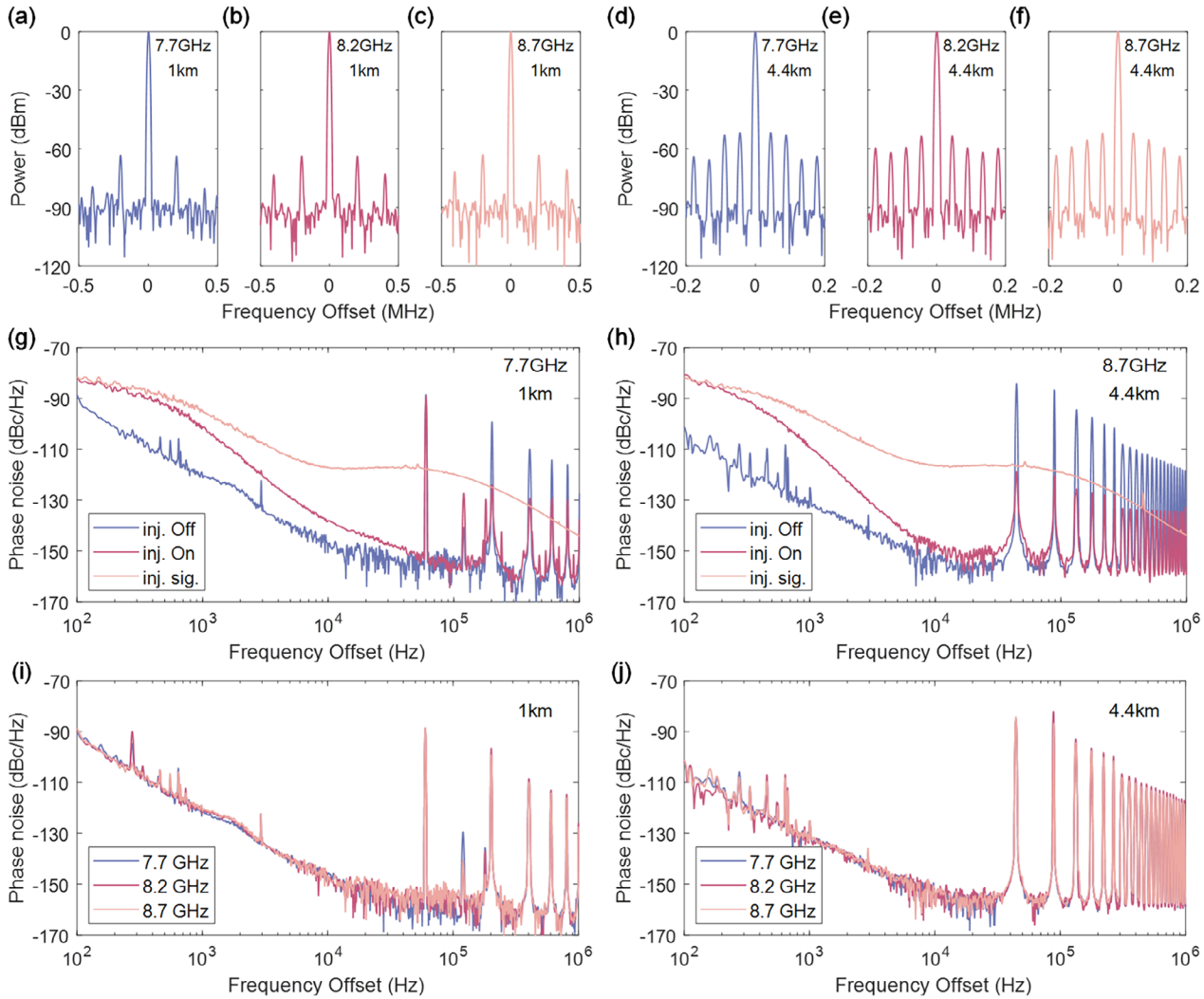

Figure 4. Deterministic PT-OEOs with ultra-low noise. a–f) Measured electrical spectra at different frequencies of PT-OEOs with 1- and 4.4-km optical fiber, respectively. g,h) Measured phase noise of the injection signal and the deterministic PT-OEOs with and without injection. i,j) Measured phase noise of the deterministic PT-OEOs without injection at different frequencies.

set, for 7.7, 8.2, and 8.7 GHz, respectively. In the 4.4 km case, the phase noises are −126.2, −125.3, and −127.7 dBc Hz^{-1} at 1 kHz frequency offset, and −156.5, −158.1, and −158.6 dBc Hz^{-1} at 10 kHz frequency offset, for the three frequencies, respectively. Notably, our deterministic PT-OEO's phase noise is comparable to that of traditional and effective microwave filter based single-loop OEO (see supporting information). Our meticulous engineering ensures that phase noise remains at exceptionally low levels in both cases, underscoring the reliability and precision of our one-shot injection configurations. This superior performance in phase noise establishes a new benchmark for stability and accuracy in optical oscillators, making our method an ideal choice for applications requiring frequency tunable and ultra-low noise sources. It is worth noting that further improvements in phase noise and frequency stability can be achieved by employing longer optical fibers,[13] electrical amplifiers with lower noise figures,[37] enhanced thermal and vibration stabilization systems,[38] phase locked loops,[35] and noise cancelation techniques.[39]

3. Discussion

A comparison of the deterministic PT-OEO presented in this work with other tunable or ultralow-phase-noise OEOs is shown in **Table 1**. The phase noises of our deterministic PT-OEOs exceed that of the tunable PT-OEO[20] and outperforms the PT-OEO with the best phase noise,[13] which utilizes a length of 9.1 km optical fiber. Furthermore, the SMSRs of our deterministic PT-OEOs are also superior to these PT-OEOs due to the utilization of shorter optical fiber, providing additional benefits in terms of thermal and vibration stability. The phase noise performances of our work also exceed traditional non-tunable single or dual-loop OEOs[35,37] with a narrowband electrical filter and similar lengths of optical fiber. Although the phase noise and SMSR reported for the OEO in Ref[39] is the best in Table 1, it involves multiple noise and side mode suppression techniques and is not directly tunable. The phase noise and SMSR of the tunable output signal from the OEO-based frequency synthesizer in Ref[39] are generally worse than this work. Although the OEO with the recorded

Table 1. Performance comparison of OEO.

References	Technical approaches	Tunablity	Fiber [km]	SMSR [dB]	PN@1kHz [dBc Hz^{-1}]	PN@10kHz [dBc Hz^{-1}]
[37]	single-loop OEO	No	1	N/A	−123	−145.8
[35]	dual-loop OEO	No	4.68	71	−124	−151
[33]	single-loop OEO	No	16	N/A	−145[a)]	−163[b)]
[39]	injection locked single-loop OEO	No	4.4	85	−127.2	−153.1
[39]	injection locked single-loop OEO + DDS +PLL	Yes	4.4	65	−115.3	−130
[40]	single-loop OEO + tunable YIG	Yes	0.5	70	−75[a)]	−116
[13]	PT-OEO	No	9.166	26	−115[a)]	−142
[20]	PT-OEO + tunable MPF	Yes	7	53	−95[a)]	−134
This work	PT-OEO with one-shot injection	Yes	1	63.8	−120.3	−149.9
			4.4	52	−127.7	−158.6

[a)] data are read from the figures; [b)] The frequency offset is 6 kHz. SMSR: side-mode suppression ratio; PN, phase noise; N/A, not available; DDS, direct digital frequency synthesizer; PLL, phase locked loop; YIG, yttrium iron garnet filter; MPF, microwave photonic filter.

−163 dBc Hz^{-1} at 6 kHz frequency offset[33] has a lower phase noise in low frequency offset than our work, the phase noise at 10 kHz offset is deteriorated by the 16 km optical fiber. Also, stabilizing such a lengthy optical fiber requires significantly more effort. It is worth noting that all these tunable OEOs require complicated tunable structures, such as tunable optical/microwave filters[20,40] or frequency conversion devices,[39] to change the frequency of their output signals. In contrast, in our case, tunability is achieved without the need for any extra structures.

4. Conclusion

In conclusion, we have successfully realized a deterministic PT-symmetric photonic oscillator with the aid of a one-shot injection signal, validated on an OEO platform. The injection locking technique effectively alters the gain spectrum of the system, amplifying the gain difference and eliminating the randomness of the oscillation frequency. This has enabled the achievement of single-mode oscillation signals ranging from 1.8 to 9 GHz with a high SMSR of 63.8 dB. Importantly, the one-shot nature of our method ensures that the phase noise of the oscillation signal remains unaffected by the injection signal, resulting in an ultra-low phase noise of −158.6 dBc Hz^{-1} at 10 kHz. The combination of PT-symmetry with the one-shot injection technique opens up new avenues for future research on optical and electrical oscillators, potentially leading to the development of high-performance and robust photonic devices for various applications such as signal generation and sensing.

5. Experimental Section

Gain Spectrum of a PT-OEO with Injection Signal: Theoretically, the n_{th} longitudinal modes in a multimode OEO with two geometrically identical coupled resonant cavities, as shown in Figure 1b, can be described by a pair of coupled differential equations in the time domain.[2] With an external injection signal, the coupled differential equations can be written as

$$\begin{aligned}\frac{da_n}{dt} &= -j\omega_n a_n + \gamma'_{a_n} a_n + j\kappa b_n + \gamma_{\text{inj,a}} c_m \\ \frac{db_n}{dt} &= -j\omega_n b_n + \gamma'_{b_n} b_n + j\kappa a_n + \gamma_{\text{inj,b}} c_m,\ (n = 1, 2, 3\ldots)\end{aligned} \tag{3}$$

where a_n and b_n are the n_{th} longitudinal modes in each cavity, c_m is the injection signal at the m_{th} mode, ω_{a_n} and ω_{b_n} are their angular frequencies, κ is the coupling coefficient between the two cavities, which is a fixed value defined by the balanced photodiode (BPD), γ_{a_n} and γ_{b_n} denote the intrinsic gain coefficients of the n_{th} longitudinal modes in each non-injected cavity, respectively, and $\gamma_{\text{inj,a}}$ and $\gamma_{\text{inj,b}}$ represent the gain coefficients induced by the injection signal, respectively. Suppose a_m, b_m, and c_m have the same phase, Equation (3) can be rewritten by combining the two gain terms.

$$\begin{aligned}\frac{da_n}{dt} &= -j\omega_n a_n + \gamma'_{a_n} a_n + j\kappa b_n \\ \frac{db_n}{dt} &= -j\omega_n b_n + \gamma'_{b_n} b_n + j\kappa a_n,\ (n = 1, 2, 3\ldots)\end{aligned} \tag{4}$$

Since the two cavities share the same electrical devices, the gain spectra are similar but with a different splitting ratio k and $k-1$. Thus, the gain coefficients in Equation (4) are given by

$$\begin{aligned}\gamma'_{a_n} &= \frac{1}{\tau}\left(\ln G_n + \delta_{m,n}\ln G_{\text{inj}} + \ln k\right) \\ \gamma'_{b_n} &= \frac{1}{\tau}\left(\ln G_n + \delta_{m,n}\ln G_{\text{inj}} + \ln(1-k)\right)\end{aligned} \tag{5}$$

where k ($0 \le k \le 1$) is the splitting ratio of the polarization beam splitter (PBS) controlled by a (PC, PC2) before it, G_n is the injection-free intrinsic loop gain spectrum of the gain cavity with $k = 1$, τ is the loop delay, G_{inj} is the gain induced by the external injection, which is determined by the amplitudes of a_m, b_m, and c_m, and $\delta_{m,n}$ is the Kronecker Delta. Compared to a single-loop OEO, injection and power splitting terms are added in Equation (5). As the two cavities have identical geometry, the longitudinal modes of both cavities share the same ω_n, that is, $\omega_{a_n} = \omega_{b_n} = \omega_n$. Solving Equation (4), one can obtain the angular frequencies of the coupled resonant cavity $\omega_n^{(1)}$ and $\omega_n^{(2)}$

$$\omega_n^{(1,2)} = \omega_n - i\frac{\gamma'_{a_n} + \gamma'_{b_n}}{2} \pm \sqrt{\kappa^2 - \left(\frac{\gamma'_{a_n} - \gamma'_{b_n}}{2}\right)^2} \tag{6}$$

Since γ'_{a_n} and γ'_{b_n} shares the same gain spectrum but are different in the $\ln k$ and $\ln(1-k)$ terms, one can tune k to meet the PT-symmetry condition. Then we have $\gamma'_{a_n} = -\gamma'_{b_n} = \gamma'_n$ and $\gamma'_n > \kappa$. Equation (6) can be simplified as

$$\omega_n^{(1,2)} = \omega_n \pm ig_n \tag{7}$$

where $g_n = \sqrt{\gamma_n'^2 - \kappa^2}$ is the gain spectrum under PT-symmetry condition. The oscillation modes in each cavity a_n and b_n share the same real frequency ω_n but have opposite gains $\pm g_n$. The b_n modes are suppressed owing to the presence of negative gains, whereas a_n modes with positive gains exhibit a sharpened gain spectrum reminiscent of a multi-passband filter.

Frequency Domain Saturated Absorption of the Mach-Zehnder Modulator: Suppose two signals at two different frequencies are fed into a Mach-Zehnder modulator (MZM) biased at the quadrature point. The electrical field of the output signal of the MZM is given by

$$x_{out}(t) \propto \cos\left(\beta_i \cos(\omega_i t) + \beta_j \cos\left(\omega_j t\right) + \frac{\pi}{2}\right) \tag{8}$$

where $\beta_i = 2\pi V_i/V_\pi$, $\beta_j = 2\pi V_j/V_\pi$ are the modulation indices of the electrical signal at each frequency, respectively. V_i, V_j and ω_i, ω_j are their voltages and angular frequencies, respectively, and V_π is the half-wave voltage of the MZM. Then $x_{out}(t)$ can be expanded as

$$x_{out}(t) \propto \sin(\beta_i \cos(\omega_i t)) \cos\left(\beta_j \cos\left(\omega_j t\right)\right) + \cos(\beta_i \cos(\omega_i t)) \sin\left(\beta_j \cos\left(\omega_j t\right)\right) \tag{9}$$

Since $\beta_i \ll 1$, so the ω_i terms can be simplified as $\cos(\beta_i \cos(\omega_i t)) \approx J_0(\beta_i)$ and $\sin(\beta_i \cos(\omega_i t)) \approx 2J_1(\beta_i)\cos(\omega_i t)$. Thus Equation (9) can be rewritten as

$$x_{out}(t) \propto 2J_1(\beta_i)\cos(\omega_i t)\cos\left(\beta_j \cos\left(\omega_j t\right)\right) + J_0(\beta_i)\sin\left(\beta_j \cos\left(\omega_j t\right)\right) \tag{10}$$

Using Jacobi expansion to the ω_j terms and extracting only the first-order frequency components, Equation (10) can be written as

$$x_{out}(t) \propto J_0\left(\beta_j\right) J_1(\beta_i)\cos(\omega_i t) + J_0(\beta_i) J_1\left(\beta_j\right)\cos\left(\omega_j t\right) \tag{11}$$

At this point, we obtain Equation (1) in the main text.

Simulation of the OEO Dynamics: The dynamics of the OEO can be calculated using a quasi-linear model adapted from a previous work.[36] The complex signal of the OEO was calculated roundtrip by roundtrip, assuming that the signal remains constant within each roundtrip and evolves in the subsequent roundtrip. The input signal for each roundtrip is the RF signal applied to the MZM, and the output signal was obtained after the input signal is processed by photodetection, amplification, and spectral shaping steps. The input signal is given as $V_{in}(t, T) = A_{in,l}(T)\exp(-j\omega_{in}t)$, where ω_c is the central modulation frequency, $A_{in,l}(T) = |A_{in,l}(T)|\exp(j\phi_{in,l}(T))$ is the slow varying amplitude complex envelope, T is the slow time scale within the time of one roundtrip τ, t is the fast time scale on the order of $2\pi/\omega_c$, and l indicates the number of roundtrips. Both t and l represent the total evolution time of the signal with the relation $t = l \cdot \tau$. Since the PT-OEO involves a large number of modes, the ripples in the frequency response of a broadband microwave photonic link must be considered. For simplicity, we assume the frequency responses of the MZM, the PD, and the amplifier are homogenous within the simulation bandwidth. Thus, the signal after passing through these devices can be expressed as $A_{amp,l}(T) = A_{in,l}(T) \cdot \eta$, where η represents the efficiency of the photonic link. We treat the ripples of the frequency response of the photonic link as an additional device (referred to hereafter as "device F") with a frequency response $H(\omega)$. Only frequencies satisfying the $f = k \cdot FSR$ ($k = 1, 2, 3 \ldots$) condition should be considered in the OEO, so $H(\omega)$ can be written as H_n. For a non-PT single loop OEO, $H_n = \exp(\gamma_n T_{loop})$. We introduce small ripples in the frequency response of device F for a common filterless single-loop OEO. For simplicity, we assume there are only two different peaks with slightly different maximum transmissions. For the PT-OEO, H_n is changed by PT-symmetry. Assuming the two PDs in the BPD have identical frequency responses, we can derive a frequency response with a shape similar to that of the non-PT-OEO, except the amplitude of the ripples is amplified by PT-symmetry. Therefore, the signal after passing through device F can be written as $A_{F,l}(T) = \mathcal{F}^{-1}\{\sum_k [\mathcal{F}(A_{amp,l}(T))_k H_k]\}$, where $\mathcal{F}$ and $\mathcal{F}^{-1}$ denote Fourier and inverse Fourier transforms, respectively, and $\mathcal{F}()_k$ represents the k_{th} Fourier component. The output signal $A_{F,l}(T)$ then serves as the input signal $A_{in,l+1}$ in the subsequent roundtrip for the non-injected OEO, while $A_{in,l+1} = A_{F,l}(T) + A_{injection}(T)$ for the injection locked OEO.

Supporting Information

Supporting Information is available from the Wiley Online Library or from the author.

Acknowledgements

H.Y., S.L., and M.L. contributed equally to this work. This work was supported in part by the National Natural Science Foundation of China under Grants 62205145 and 62271249; in part by the National Key Research and Development Program of China under Grant 2022YFB2802700; in part by the Natural Science Foundation of Jiangsu Province under Grant BK20220887; in part by the Fundamental Research Funds for the Central Universities under Grant NJ2023020 and NI2023003.

Conflict of Interest

The authors declare no conflict of interest.

Data Availability Statement

The data that support the findings of this study are available from the corresponding author upon reasonable request.

Keywords

microwave photonics, optical resonators, optoelectronic oscillators, oscillators, parity-time symmetry

Received: June 17, 2024
Revised: November 1, 2024
Published online:

[1] C. M. Bender, S. Boettcher, *Phys. Rev. Lett.* **1998**, *80*, 5243.
[2] R. El-Ganainy, K. G. Makris, D. N. Christodoulides, Z. H. Musslimani, *Opt. Lett.* **2007**, *32*, 2632.
[3] C. E. Rueter, K. G. Makris, R. El-Ganainy, D. N. Christodoulides, M. Segev, D. Kip, *Nat. Phys.* **2010**, *6*, 192.
[4] H. Hodaei, M.-A. Miri, M. Heinrich, D. N. Christodoulides, M. Khajavikhan, *Science* **2014**, *346*, 975.
[5] M. Brandstetter, M. Liertzer, C. Deutsch, P. Klang, J. Schoeberl, H. E. Tuereci, G. Strasser, K. Unterrainer, S. Rotter, *Nat. Commun.* **2014**, *5*, 4034.
[6] W. Liu, M. Li, R. S. Guzzon, E. J. Norberg, J. S. Parker, M. Lu, L. A. Coldren, J. Yao, *Nat. Commun.* **2017**, *8*, 15389.
[7] B. Peng, S. K. Oezdemir, F. Lei, F. Monifi, M. Gianfreda, G. L. Long, S. Fan, F. Nori, C. M. Bender, L. Yang, *Nat. Phys.* **2014**, *10*, 394.
[8] L. Chang, X. Jiang, S. Hua, C. Yang, J. Wen, L. Jiang, G. Li, G. Wang, M. Xiao, *Nat. Photonics* **2014**, *8*, 524.

[9] F. Gu, F. Xie, X. Lin, S. Linghu, W. Fang, H. Zeng, L. Tong, S. Zhuang, *Light Sci. Appl.* **2017**, *6*, e17061.
[10] G. Zhao, S. K. Ozdemir, T. Wang, L. Xu, E. King, G.-L. Long, L. Yang, *Sci. Bull.* **2017**, *62*, 875.
[11] C. Kim, X. Lu, D. Kong, N. Chen, Y. Chen, L. K. Oxenløwe, K. Yvind, X. Zhang, L. Yang, M. Pu, J. Xu, *eLight* **2024**, *4*, 6.
[12] J. Schindler, A. Li, M. C. Zheng, F. M. Ellis, T. Kottos, *Phys. Rev. A* **2011**, *84*, 040101.
[13] J. Zhang, J. Yao, *Sci. Adv.* **2018**, *4*, eaar6782.
[14] Y. Liu, T. Hao, W. Li, J. Capmany, N. Zhu, M. Li, *Light Sci. Appl.* **2018**, *7*, 38.
[15] Z. Fan, W. Zhang, Q. Qiu, J. Yao, *J. Lightwave Technol.* **2020**, *38*, 2127.
[16] P. Li, Z. Dai, Z. Fan, L. Yan, J. Yao, *Opt. Lett.* **2020**, *45*, 3139.
[17] C. Teng, X. Zou, P. Li, C. Xie, Y. Sun, W. Pan, L. Yan, *IEEE Photonics Technol. Lett.* **2020**, *32*, 47.
[18] J. Zhang, L. Li, G. Wang, X. Feng, B.-O. Guan, J. Yao, *Nat. Commun.* **2020**, *11*, 3217.
[19] L. Wang, Y. Liu, Y. Yu, X. Zhang, in *2023 Optical Fiber Communications Conference and Exhibition (OFC)*, San Diego, CA, USA, **2023**.
[20] J. Zhang, Y. Wang, Q. Ding, *Appl. Opt.* **2024**, *63*, 566.
[21] L. Wang, Y. Liu, Y. Yu, Y. Yu, X. Zhang, *ACS Photonics* **2023**, *10*, 2308.
[22] M. Li, T. Hao, G. Li, A. Wang, Y. Dai, W. Li, J. Capmany, J. Yao, N. Zhu, M. Li, *Nat. Commun.* **2024**, *15*, 8710.
[23] E. U. Rafailov, M. A. Cataluna, W. Sibbett, *Nat. Photonics* **2007**, *1*, 395.
[24] Z. Q. Luo, C. Liu, Y. Z. Huang, D. D. Wu, J. Y. Wu, H. Y. Xu, Z. P. Cai, Z. Q. Lin, L. P. Sun, J. Weng, *IEEE J. Sel. Top. Quantum Electron.* **2014**, *20*, 0902708.
[25] Y. Z. Wang, W. C. Huang, C. Wang, J. Guo, F. Zhang, Y. F. Song, Y. Q. Ge, L. M. Wu, J. Liu, J. Q. Li, H. Zhang, *Laser Photonics Rev.* **2019**, *13*, 1800313.
[26] K. Kurokawa, *Proc. IEEE* **1973**, *61*, 1386.
[27] R. Lang, *IEEE J. Quantum Electron.* **1982**, *18*, 976.
[28] C. J. Born, S. Yu, M. Sorel, P. J. R. Laybourn, in *Conference on Lasers and Electro-Optics*, Washington D.C., USA, **2003**.
[29] W. M. Zhou, G. Blasche, *IEEE Trans. Microwave Theory Tech.* **2005**, *53*, 929.
[30] W. Weng, E. Lucas, G. Lihachev, V. E. Lobanov, H. Guo, M. L. Gorodetsky, T. J. Kippenberg, *Phys. Rev. Lett.* **2019**, *122*, 013902.
[31] M. H. Li, L. Z. Li, J. J. Zhang, J. P. Yao, in *7th Asia Pacific Conference on Optics Manufacture (APCOM)*, Shanghai, China, **2021**.
[32] Z. J. Jiao, P. C. Zuo, L. Xue, G. F. Li, Y. Chen, *Appl. Opt.* **2022**, *61*, 9868.
[33] D. Eliyahu, D. Seidel, L. Maleki, in *2008 IEEE International Frequency Control Symposium*, Honolulu, HI, USA, **2008**.
[34] A. Martinez, Z. Sun, *Nat. Photonics* **2013**, *7*, 842.
[35] X. Wang, X. S. Yao, *IEEE Trans. Microwave Theory Tech.* **2023**, *71*, 5381.
[36] E. C. Levy, M. Horowitz, C. R. Menyuk, *J. Opt. Soc. Am. B: Opt. Phys.* **2009**, *26*, 148.
[37] O. Lelievre, V. Crozatier, P. Berger, G. Baili, O. Llopis, D. Dolfi, P. Nouchi, F. Goldfarb, F. Bretenaker, L. Morvan, G. Pillet, *J. Lightwave Technol.* **2017**, *35*, 4366.
[38] L. Bogataj, M. Vidmar, B. Batagelj, *J. Lightwave Technol.* **2016**, *34*, 885.
[39] S. Liu, X. Xu, F. Zhang, P. Liu, X. Kang, H. Yang, S. Pan, *J. Radars* **2019**, *8*, 243.
[40] G. Zhang, T. Hao, Q. Cen, M. Li, N. Shi, W. Li, X. Xiao, N. Qi, J. Dong, Y. Dai, N. Zhu, M. Li, *Opt. Express* **2023**, *31*, 16929.